Molecular Structures and Magnetic Properties of the Mixed-Ligand Complexes of Bis(hexafluoroacetylacetonato)manganese(II), -copper(II), and -zinc(II) with 4,4′-Bis(*N*-*tert*-butyl-*N*-oxylamino)-2,2′-bipyridine. Isosceles Triangular Hetero-Three-Spin Systems Consisting of Aminoxyls and Metal Ions

Akira Sakane,[†] Harumi Kumada,[†] Satoru Karasawa,[†] Noboru Koga,*[,†] and Hiizu Iwamura[‡]

Graduate School of Pharmaceutical Sciences, Kyushu University, 3-1-1 Maidashi, Higashi-ku, Fukuoka 812-8582, Japan, and National Institution for Academic Degrees, 4259 Nagatsuta, Midori-ku, Yokohama 226-0026, Japan

Received October 12, 1999

4,4′-Bis(*N*-*tert*-butyloxylamino)-2,2′-bipyridine (**4**) and its 1:1 complexes with bis(hexafluoroacetylacetonato)-manganese(II), -copper(II), and -zinc(II) were prepared. An X-ray structure analysis of free ligand **4** reveals that the molecule has a trans conformation with C_i symmetry and the aminoxyl radical center has a short contact of 2.36 Å with one of the neighboring molecules. The three 1:1 complexes have mutually similar molecular structures in which the 2,2′-bipyridine moiety has a cis conformation and serves as a bidentate ligand and coordination geometry around the metal atom is a distorted octahedron. The EPR experiments for free ligand **4** and [Zn(hfac)$_2$·**4**] in frozen solution suggested that the exchange couplings between the two aminoxyls (R) through the 2,2′-bipyridine rings are antiferromagnetic with $J_{R-R}/k_B = -19.3 \pm 0.5$ and -24.3 ± 0.4 K, respectively. Isosceles triangular three-spin models were applied to the 1:1 magnetic metal complexes to give $J_{R-M}/k_B = -19.1 \pm 0.2$ K and $J_{R-R}/k_B = -32.9 \pm 0.3$ K for [Mn(hfac)$_2$·**4**] and $J_{R-M}/k_B = +73 \pm 18$ K and $J_{R-R}/k_B = -24.5 \pm 6.5$ K for [Cu(hfac)$_2$·**4**].

Introduction

In the 1:2 mixed-ligand complexes of bis(hexafluoroacetylacetonato)manganese(II) and -copper(II), {Mn(hfac)$_2$ and Cu(hfac)$_2$}, with 4-(*N*-*tert*-butyloxylamino)pyridine, **1**, magnetic

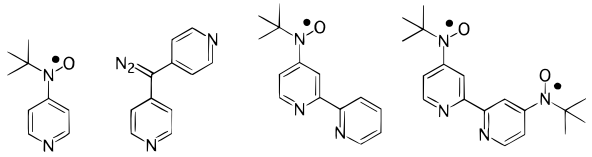

1 2 3 4

interactions between the aminoxyl radicals and the metal ions through the pyridine rings are metal-dependent: antiferromagnetic for Mn(II) and ferromagnetic for Cu(II).[1−3] On the basis of these important findings, we previously developed photochemical formations of ferri- and ferromagnetic chains from the complexes of Mn(hfac)$_2$ and Cu(hfac)$_2$ with diazodi(4-pyridyl)methane, **2**, respectively.[4,5] In this paper, we employ, in place of the pyridine, 2,2′-bipyridine ligands which are known to form bis and tris complexes with various metal ions.[6] To understand the magnetic coupling in the metal complexes with 2,2′-bipyridines carrying organic spins,[7] 4-(*N*-*tert*-butyloxylamino)-2,2′-bipyridine and 4,4′-bis(*N*-*tert*-butyloxylamino)-2,2′-bipyridine (**3** and **4**) and their 1:1 complexes with Mn(hfac)$_2$ and Cu(hfac)$_2$ were designed and prepared. Similarly, a diamagnetic metal ion, zinc(II), was used to prepare reference complexes [Zn(hfac)$_2$·**3** and **4**].[8]

Experimental Section

General Methods. Infrared spectra were measured on a Hitachi 270-30 IR spectrometer. ^{1}H NMR spectra were measured on a JEOL 270 Fourier transform spectrometer using $CDCl_3$ as solvent and referenced to TMS. FAB mass spectra (FAB MS) were recorded on a JEOL JMS-SX102 spectrometer. Melting points were obtained with a MEL-TEMP

[†] Kyushu University.
[‡] National Institution for Academic Degrees.

(1) (a) Koga, N.; Iwamura, H. In *Magnetic Properties of Organic Materials*; Lahti, P., Ed.; Marcel Dekker: New York, 1999; Chapter 30, p 629. (b) Iwamura, H.; Koga, N. *Pure Appl. Chem.* **1999**, *71*, 231.
(2) (a) Kitano, M.; Ishimaru, Y.; Inoue, K.; Koga, N.; Iwamura, H. *Inorg. Chem.* **1994**, *33*, 6012−6019. (b) Kitano, M.; Inoue, K.; Koga, N.; Iwamura, H. *J. Chem. Soc., Chem. Commun.* **1994**, 447.
(3) Ishimaru, Y.; Kitano, M.; Kumada, H.; Koga, N.; Iwamura, H. *Inorg. Chem.* **1998**, *37*, 2273.
(4) (a) Karasawa, S.; Sano, Y.; Akita, T.; Koga, N.; Itoh, T.; Iwamura, H.; Rabu, P.; Drillon, M. *J. Am. Chem. Soc.* **1998**, *120*, 10080. (b) Koga, N.; Ishimaru, Y.; Iwamura, H. *Angew. Chem., Int. Ed. Engl.* **1996**, *35*, 755.
(5) (a) Sano, Y.; Tanaka, M.; Koga, N.; Matsuda, K.; Iwamura, H.; Rabu, P.; Drillon, M. *J. Am. Chem. Soc.* **1997**, *119*, 8246. (b) Koga, N.; Iwamura, H. *Mol. Cryst. Liq. Cryst.* **1997**, *305*, 415. (c) Karasawa, S.; Tanaka, M.; Koga, N.; Iwamura, H. *Chem. Commun. (Cambridge*) **1997**, 1359.
(6) McWhinnie, W. R.; Miller, J. D. *Adv. Inorg. Chem. Radiochem.* **1969**, *12*, 135.
(7) (a) Stroh, C.; Ziessel, R. *Tetrahedron Lett.* **1999**, *40*, 4543. This paper deals with 2,2′-bipyridines carrying Ullman's nitronyl nitroxide at the 6- (and 6′-) position. Since the radical substituent is attached to the 2,2′-bipyridine unit through the carbon atom of low negative spin density, the interaction between the radical centers through the bipyridine ring is negligible. Thus the interest of these authors is different from that of the present authors. (b) Morikawa, H.; Kumada, H.; Koga, N.; Iwamura, H. To be published.
(8) The molecular structures and magnetic properties of **3** and its metal complexes have been reported recently: Kumada, H.; Sakane, A.; Koga, N.; Iwamura, H. *J. Chem. Soc., Dalton Trans.* **2000**, 911.

10.1021/ic991205f CCC: $19.00
Published on Web 05/31/2000

Table 1. Crystal Data and Structure Refinements for **4**, [Zn(hfac)$_2$·**4**], [Mn(hfac)$_2$·**4**], and [Cu(hfac)$_2$·**4**]

	4	[Zn(hfac)$_2$·**4**]	[Mn(hfac)$_2$·**4**]	[Cu(hfac)$_2$·**4**]
empirical formula	$C_{18}H_{24}N_4O_2$	$C_{28}H_{26}N_4O_6F_{12}Zn$	$C_{28}H_{26}N_4O_6F_{12}Mn$	$C_{28}H_{26}N_4O_6F_{12}Mn$
fw	328.43	807.90	797.46	806.07
a (Å)	8.349(2)	12.768(1)	12.68(2)	23.427(2)
b (Å)	9.068(2)	22.184(3)	22.052(3)	16.983(1)
c (Å)	6.700(1)	13.312(2)	13.275(6)	21.999(2)
α (deg)	108.29(2)			
β (deg)	109.18(2)	113.019(2)	111.73(6)	128.974(4)
γ (deg)	100.57(2)			
V (Å^3)	431.0(2)	3470.4(7)	3447(4)	6804.2(9)
space group	$P\bar{1}$ (No. 2)	$C2/c$ (No. 15)	$C2/c$ (No. 15)	$C2/c$ (No. 15)
Z	1	4	4	8
ρ_{calcd} (g cm^{-3})	1.273	1.546	1.536	1.246
λ (Å)	1.54178 (Cu Kα)	0.71069 (Mo Kα)	0.71069 (Mo Kα)	0.71069 (Mo Kα)
μ (cm^{-1})	6.82 (Cu Kα)	8.17 (Mo Kα)	4.93 (Mo Kα)	5.64 (Mo Kα)
R^a (F_o)	0.048	0.055	0.054	0.060
$R_w{}^a$ (F_o)	0.043	0.052	0.070	0.056
T (K)	298	296	296	296

[a] $R = \sum(||F_o| - |F_c||)/\sum|F_o|$. $R_w = [\sum w(|F_o| - |F_c|)^2/\sum w|F_o|^2]^{1/2}$.

heating block and are uncorrected. Elemental analyses were performed at the Analytical Center of Faculty of Science in Kyushu University.

X-ray Crystal and Molecular Structural Analyses. Diffraction data were collected using Cu Kα and Mo Kα radiations on Rigaku AFC5R and AFC7R four-circle diffractometers for **4** and [Mn(hfac)$_2$·**4**], respectively, and using Mo Kα radiation on a Rigaku RAXIS-IV imaging plate area detector system attached with a liquid-nitrogen cooling system for [Cu(hfac)$_2$·**4**] and [Zn(hfac)$_2$·**4**]. In RAXIS-IV, the incident radiation consisted of Mo Kα X-rays generated by a rotating-anode X-ray generator fitted with a graphite monochromator and operated at 50 kV and 40 mA. The oscillation angle used for [Zn(hfac)$_2$·**4**] and [Cu(hfac)$_2$·**4**] was 5°, and each data frame was exposed for 10 min. Totals of 46 data frames for [Zn(hfac)$_2$·**4**] and [Cu(hfac)$_2$·**4**] were collected and processed using the RAXIS control software. Pertinent crystallographic parameters and refinement data are collected in Table 1.

The structures of **4**, [Zn(hfac)$_2$·**4**], [Mn(hfac)$_2$·**4**], and [Cu(hfac)$_2$·**4**] were solved in $P\bar{1}$ (No. 2), $C2/c$ (No. 15), $C2/c$ (No. 15), and $C2/c$ (No. 15), respectively, by direct methods,[11] and refinement converged using a full-matrix least-squares method of the teXsan[12] crystallographic software package (version 1.9). All non-hydrogen atoms were refined anisotropically; hydrogen atoms were included at standard positions (C−H 0.96 Å, C−C−H 120°) and refined isotropically using a rigid model.

EPR Spectra and Magnetic Measurements. EPR spectra were recorded on a Bruker ESP300 X-band (9.4 GHz) spectrometer equipped with a Hewlett-Packard 5350B microwave frequency counter. An Air Products LTD-3-110 liquid helium transfer system was attached for the low-temperature measurements. Sample solutions were placed in 5 mm o.d. quartz tubes, degassed by three freeze-and-thaw cycles, and sealed.

Magnetic susceptibility data were obtained on Quantum Design MPMS$_2$ (0−10 kOe) and MPMS (0−50 kOe) SQUID magnetometer/susceptometers. The data were corrected for the diamagnetic contribution in the range -3.7×10^{-5} to -6.7×10^{-5} emu·G of sample capsules and holding straws used. The diamagnetic contributions of the samples were estimated by Pascal's constants.

Preparation of the Ligands and the Metal Complexes. Unless otherwise stated, preparative reactions were carried out under a high-purity dry nitrogen atmosphere. Diethyl ether and dichloromethane were distilled from sodium benzophenone ketyl and over calcium hydride, respectively. Bis(hexafluoroacetylacetonato)manganese(II), -copper(II), -zinc(II) {M(hfac)$_2$, M = Mn(II), Cu(II), and Zn(II)}, 2-methyl-2-nitrosopropane,[13] and 4,4′-dibromo-2,2′-bipyridine[14] were prepared and purified by the literature procedures.

4,4′-Bis(*N*-*tert*-butylhydroxylamino)-2,2′-bipyridine. To a solution of 2.2 g (9.9 mmol) of 4, 4′-dibromo-2,2′-bipyridine in 100 mL of dry ether at −78 °C was added 12.8 mL of a 1.6 M solution of *n*-butyllithium in *n*-hexane. After stirring for 30 min, a solution of 0.85 g (9.9 mmol) of 2-methyl-2-nitrosopropane in 15 mL of ether was added dropwise. The reaction mixture was stirred for 1 h at −78 °C. After the usual workup, the precipitate was chromatographed on aluminum oxide with dichloromethane as eluent to give 0.57 g (2.5 mmol, 25.3% yield) of the hydroxyamine as a white solid: mp 245−248 °C; IR (KBr) ν 3203 cm^{-1}; ^{1}H NMR (270 MHz, $CDCl_3$) δ 1.19 (s, 9H), 7.15 (dd, J = 2.0 and 5.4 Hz, 1H), 8.22 (d, J = 2.0 Hz, 1H), 8.43 (d, J = 5.4 Hz, 1H), 8.70 (s, 1H); FAB mass (in *m*-NBA matrix) 331 (M + 1). As this hydroxyamine was easily oxidized by air during a crystallization, it was used for oxidation reaction without further purification.

4,4′-Bis(*N*-*tert*-butyl-*N*-oxylamino)-2,2′-bipyridine (4). To a solution of 0.025 g (0.11 mmol) of dihydroxyamine in 20 mL of dry ether was added 0.33 g of freshly prepared Ag_2O. The suspension was stirred for 30 min and filtered: mp 161−162 °C; FAB mass (in *m*-NBA matrix) 331 (M + 3). Anal. Calcd for $C_{18}H_{24}N_4O_2$: C, 65.83; H, 7.37; N, 17.06. Found: C, 65.72; H, 7.41; N, 16.76. EPR (CH_2Cl_2): g = 2.0068, $a_N/2$ = 5.6 G.

4,4′-Bis(*N*-*tert*-butyloxylamino)-2,2′-bipyridinebis(hexafluoroacetylacetonato)manganese(II) [Mn(hfac)$_2$·4]. A solution of 0.15 g (0.3 mmol) of bis(hexafluoroacetylacetonato)manganese(II)·2H$_2$O in 40 mL of *n*-heptane was heated to reflux for 15 min and cooled to room temperature, and a solution of **4** (0.6 mmol) in 10 mL of ether was added. The solution was left under a stream of nitrogen gas. Manganese complex was obtained as orange plates in 27% yield: mp 197−193 °C. Anal. Calcd for $C_{28}H_{26}N_4O_6F_{12}Mn$: C, 42.17; H, 3.29; N, 7.03. Found: C, 42.42; H, 3.30; N, 7.12.

4,4′-Bis(*N*-*tert*-butyloxylamino)-2,2′-bipyridinebis(hexafluoroacetylacetonato)copper(II) [Cu(hfac)$_2$·4]. This was prepared in a manner similarly to [Mn(hfac)$_2$·**4**] using Cu(hfac)$_2$ in place of Mn(hfac)$_2$. Brown blocks were obtained in 31% yield: mp 185−187 °C. Anal. Calcd for $C_{28}H_{26}N_4O_6F_{12}Cu$: C, 41.72; H, 3.25; N, 6.95. Found: C, 41.79; H, 3.23; N, 7.02.

4,4′-Bis(*N*-*tert*-butyloxylamino)-2,2′-bipyridinebis(hexafluoroacetylacetonato)zinc(II) [Zn(hfac)$_2$·4]. This was prepared in a manner similarly to [Mn(hfac)$_2$·**4**] using Zn(hfac)$_2$ in place of Mn(hfac)$_2$. Orange needles were obtained in 15% yield: mp 178−180 °C. Anal. Calcd for $C_{28}H_{26}N_4O_6F_{12}Zn$: C, 41.63; H, 3.24; N, 6.93. Found: C, 41.88; H, 3.28; N, 7.21.

(9) (a) Kahn, O. *Molecular Magnetism*, VCH: New York, 1993; Chapter 10. (b) Woo, H. Y.; So, H.; Pope, M. T. *J. Am. Chem. Soc.* **1996**, *118*, 621.
(10) Fujita, J.; Tanaka, M.; Suemune, H.; Koga, N.; Matsuda, K.; Iwamura, H. *J. Am. Chem. Soc.* **1996**, *118*, 9347.
(11) SHELEX86 for **4**, SIR92 for [Zn(hfac)$_2$·**4**] and [Mn(hfac)$_2$·**4**], and SAPI91 for [Cu(hfac)$_2$·**4**].
(12) Crystal Structure Analysis Package, Molecular Structure Corporation (1985 and 1992).
(13) Stowell, J. C. *J. Org. Chem.* **1971**, *36*, 3055.
(14) (a) Maerker, G.; Case, F. H. *J. Am. Chem. Soc.* **1958**, *80*, 2745. (b) Wenkert, D.; Woodward, R. B. *J. Org. Chem.* **1983**, *48*, 283.

Table 2. Selective Bond Lengths (Å), Bond Angles (deg), and Dihedral Angles (deg) for [Zn(hfac)$_2$·**4**], [Mn(hfac)$_2$·**4**], and [Cu(hfac)$_2$·**4**]

[Zn(hfac)$_2$·**4**]		[Mn(hfac)$_2$·**4**]		[Cu(hfac)$_2$·**4**]			
			Bond Lengths (Å)				
Zn−O2	2.093(2)	Mn−O2	2.155(3)	Cu−O2	1.961(5)	Cu−O3	2.308(5)
Zn−O3	2.130(3)	Mn−O3	2.160(4)	Cu−O5	1.962(5)	Cu−O6	2.340(5)
Zn−N2	2.135(3)	Mn−N2	2.240(4)	Cu−N2	1.998(6)	Cu−N4	1.992(6)
			Angles (deg)				
O2−Zn−N2	166.32(10)	O2−Mn−N2	161.0(1)	O2−Cu−N2	172.8(2)	O2−Cu−N4	94.9(2)
O2−Zn−N2′	93.0(8)	O2−Mn−N2′	92.1(1)	O3−Cu−N2	99.1(2)	O3−Cu−N4	89.9(2)
O3−Zn−N2	96.5(1)	O3−Mn−N2	87.8(1)	O5−Cu−N2	95.0(2)	O5−Cu−N4	173.3(2)
O3−Zn−N2′	96.4(6)	O3−Mn−N2′	97.7(1)	O6−Cu−N2	87.6(2)	O6−Cu−N4	99.4(2)
O2−Zn−O3	84.14(9)	O2−Mn−O3	94.2(1)	O2−Cu−O3	86.4(2)	O5−Cu−O6	85.3(2)
N2−Zn−N2′	77.7(1)	N2−Mn−N2′	73.7(2)	N2−Cu−N4	80.6(2)		
			Dihedral Angles (deg)				
O1N1C3−C1C3C5	16.11	O1N1C3−C1C3C5	16.83	O1N1C3−C1C3C5	33.09	O2N2C12−C10C12C14	15.35
N2ZnN2′−N2C2C4	6.50	N2MnN2′−N2C2C4	5.89	N2CuN4−N2C2C4	3.40	N2CuN4−N4C16C18	3.17
N2ZnO2′−N2C2C4	12.41	N2MnO2′−N2C2C4	13.13	N2CuO5−N2C2C4	8.40	N2CuO2−N4C16C18	5.21

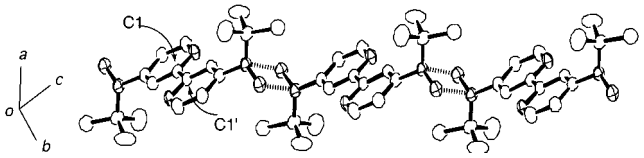

Figure 1. Ball-and-stick model of the crystal structure for **4**. Broken lines indicate short contacts of 2.36 Å.

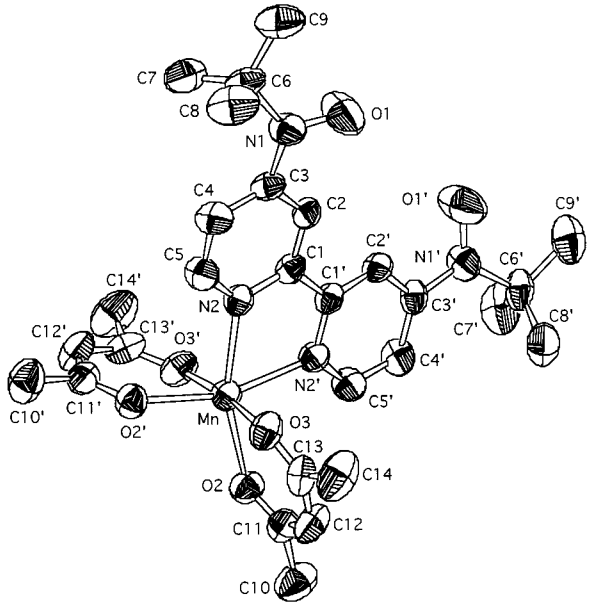

Figure 2. ORTEP drawing of the molecular structure for [Mn(hfac)$_2$·**4**] using 50% probability ellipsoids.

Results

X-ray Molecular and Crystal Structures. The molecular and crystal structures of the metal-free ligand **4** and the 1:1 mixed-ligand complexes of {M(hfac)$_2$, M = Zn(II), Mn(II), and Cu(II)} with **4** were investigated by X-ray single-crystal analysis. Crystallographic data and experimental parameters for **4** and [Zn-, Mn-, and Cu(hfac)$_2$·**4**] are summarized in Table 1. Selected bond lengths, angles, and dihedral angles for metal complexes are given in Table 2.

The crystal packing of **4** and the molecular structure of [Mn- and Cu(hfac)$_2$·**4**] revealed by X-ray analysis are shown in Figures 1, 2, and 3, respectively.

(A) Biradical 4. A metal-free ligand **4** has a C_i symmetry at the midpoint of the C(1)−C(1′) bond (Figure 1). In the molecular structure, the nitrogen atoms of the two pyridine rings are directed to opposite sides and both planes are coplanar. The dihedral angle between aminoxyl plane and 2,2′-bipyridine ring amounts to 38.9°. As observed in the crystal structure of Figure 1, the molecules are aligned in the [1.1.1] direction by a distance of 2.36 Å between O(1) of the aminoxyl center and N(1′) of the neighboring molecule. The observed distance of 2.36 Å shorter than the van der Waals contact (3.07 Å) suggests the production of extremely strong antiferromagnetic interaction in the crystal.

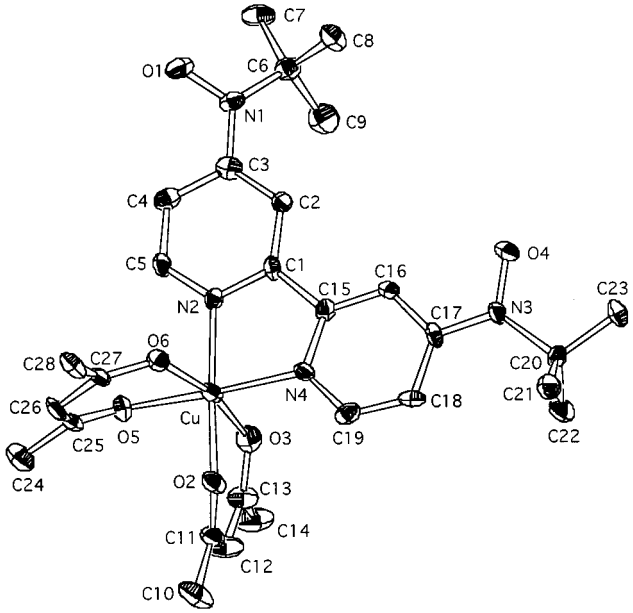

Figure 3. ORTEP drawing of the molecular structure for [Cu(hfac)$_2$·**4**] using 50% probability ellipsoids.

(B) [Mn-, Cu-, and Zn(hfac)$_2$·4]. Among the molecular structures of three mixed-ligand metal complexes, [Mn(hfac)$_2$·**4**] and [Zn(hfac)$_2$·**4**] have a C_2 symmetry axis through the midpoint of the C(1)−C(1′) bond and the metal ion, and [Cu(hfac)$_2$·**4**] has no symmetry axis. The NO bonds of the aminoxyls are directed to each other by distances of 5.87 and 5.82 Å between O atoms for Mn and Zn complexes, respectively, while they are directed to the same direction in the Cu complex. The coordination geometries of three complexes are distorted octahedra. As listed for bond lengths around metal ions in Table 2, the elongation axis in [Cu(hfac)$_2$·**4**] is through O(3)−Cu−O(6), and it is assumed to be a *z* axis. The dihedral

angles between the planes of the bipyridine and the aminoxyl groups are 16.1° and 16.1° for [Zn(hfac)$_2$·**4**], 16.8° and 16.8° for [Mn(hfac)$_2$·**4**], and 33.1° and 15.4° for [Cu(hfac)$_2$·**4**]. The crystal structures of [Mn(hfac)$_2$·**4**] and [Zn(hfac)$_2$·**4**] are also similar to each other. The mixed-ligand complex molecules are relatively separated, and the nearest contact between them is found to be 4.7 and 4.5 Å of NO−NO in the Mn and Zn complexes, respectively. On the other hand, the copper complex has a head-to-tail dimer structure in which both planes are slightly slipped with respect to each other. The average distance between two bipyridine planes is 3.63 Å, and the nearest contact is 3.16 Å between O(1) of aminoxyl and C(18) of bipyridine ring. The dimer is separated well, and the observed structure is close to the one for [Cu(hfac)$_2$·**3**] reported recently.[8]

Magnetic Data and Analyses

(A) EPR Spectra. EPR spectra of **4** and [Zn(hfac)$_2$·**4**] in toluene at room temperature showed five lines with $a_N/2 = 5.6$ and 5.1 G due to nitrogen nuclei, respectively. Their spectra in frozen solution of toluene at a cryogenic temperature were similar to each other. A characteristic set of fine structures with $|D/hc| = 0.0054$ and 0.0094 cm^{-1} due to a triplet state were observed for **4** and [Zn(hfac)$_2$·**4**], respectively. The signal due to the $\Delta m_s = \pm 2$ transition at 168.4 mT was also observed for **4**. When the temperature (T) was raised from 6 K, the triplet signal intensities (I) for **4** and [Zn(hfac)$_2$·**4**] increased, reached maxima at ca. 24 and 30 K, respectively, and then decreased above these temperatures. The temperature dependence of the triplet signal intensities indicates that the observed triplets are thermally excited states which lie above singlet ground states. Energy differences (ΔE_{S-T}) between the singlet and triplet states are estimated to be $\Delta E_{S-T} = 76.8 \pm 2.2$ and 96.6 ± 1.4 cal/mol ($J/k_B = -19.3 \pm 0.5$ and -24.3 ± 0.4 K), respectively, by fitting the Bleaney−Bowers equation (eq 1)[15] to the experimental I vs $1/T$ plots.

$$I = \frac{C}{T}\frac{1}{3 + \exp(-J/k_BT)} \qquad (1)$$

(B) Paramagnetic Susceptibility Measurements. The molar magnetic susceptibility data of crystalline samples of **4** and its metal complexes, [Zn-, Mn-, and Cu(hfac)$_2$·**4**], were obtained on SQUID magneto/susceptometers in the temperature range 2−300 K at a constant field of 5 kOe. The temperature dependence of molar magnetic susceptibility (χ_{mol}) for [Zn-, Mn-, and Cu(hfac)$_2$·**4**] is shown in Figure 4, panels a, b, and c, respectively. The basic structures for the 1:1 metal complexes with **4** should be described by a triangular three-spin system as shown in Scheme 1, where local spins and exchange coupling parameters are denoted S_{A1}, S_{A2}, and S_{A3}, and J_1, J_2, and J_3, respectively.[9,10] Previously, the magnetic data for 1:2 complexes [Mn(hfac)$_2$·**1**$_2$] and [Cu(hfac)$_2$·**1**$_2$] were analyzed as a linear three-spin system where S_{A1}, S_{A2}, and $S_{A3} = S_M$ are aminoxyl, aminoxyl, and metal ion, respectively, and $J_1 = J_2$ by symmetry and $J_3 = 0$ by neglecting the non-neighbor interaction mediated by the metal ion.[2,3] Thus the obtained $\chi_{mol}T$ vs T curves for [Mn(hfac)$_2$·**4**] and [Cu(hfac)$_2$·**4**] were analyzed quantitatively on the basis of an isosceles triangular three-spin model. For spin Hamiltonian

$$H = -2J(S_{A1}S_M + S_MS_{A2} + \alpha S_{A1}S_{A2}) \qquad (2)$$

(15) Bleaney, B.; D. Bowers, K. *Proc. R. Soc. London* **1952**, *A214*, 451.

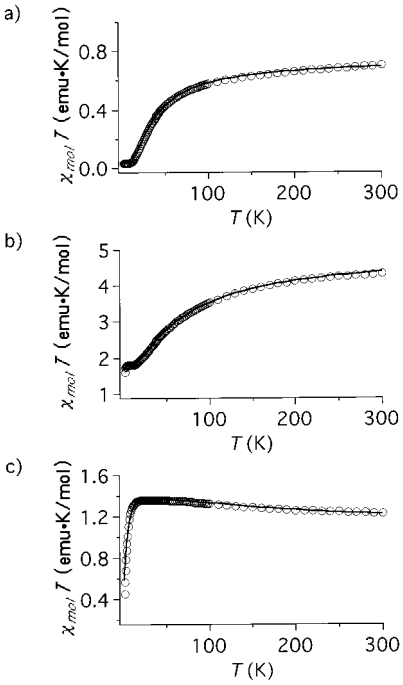

Figure 4. The plots of $\chi_{mol}T$ vs T for (a) [Zn(hfac)$_2$·**4**], (b) [Mn(hfac)$_2$·**4**], and (c) [Cu(hfac)$_2$·**4**]. The solid curves are theoretical ones as described in text.

Scheme 1

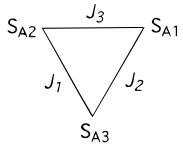

$S_{A3} = S_M$, $J_1 = J_2 = J$, and $J_3 = \alpha J$ in Scheme 1 in view of the X-ray molecular and crystal structure.

(B-1) Biradical 4. The χ_{mol} value at 300 K for **4** is 0.085 emu·K·mol^{-1} and extremely small compared with a theoretical one (0.75) calculated by two isolated spins with $S = {}^1/_2$. When an intermolecular short contact (2.36 Å) revealed by X-ray analysis is taken into account, the observed small χ_{mol} value is due to the strong antiferromagnetic interaction between the molecules.

(B-2) [Zn(hfac)$_2$·4]. In the $\chi_{mol}T$ vs T plot (Figure 4a) for **[Zn(hfac)$_2$·4]**, the $\chi_{mol}T$ value at 300 K is 0.702 emu·K·mol^{-1}, which is in good agreement with the theoretical one ($\chi_{mol}T = 0.75$ emu·K·mol^{-1}) for an isolated two-spin system with $S = {}^1/_2$. As the temperature was decreased, the $\chi_{mol}T$ value decreased gradually to nearly zero at 10 K. A two-spin model including the Curie−Weiss constant (θ) for intermolecular interactions and the fraction (f) for an impurity with $S = {}^1/_2$ was assumed and eq 3 fitted to the experimental data to give $J/k_B = -28.23 \pm 0.03$ K, $\theta = -9.58 \pm 0.43$ K, $f = 0.04 \pm 0.01$, and $g = 2.00 \pm 0.01$. The theoretical curve is represented by a solid line in Figure 4a.

$$\chi_{mol}T = \frac{Ng^2\beta^2T}{k_B(T-\theta)}\frac{2}{3 + \exp(-J_{R-R}/k_BT)}(1-f) + \frac{Ng^2\beta^2}{k_B(T-\theta)}f \qquad (3)$$

(B-3) [Mn(hfac)$_2$·4]. A $\chi_{mol}T$ value of 4.33 emu·K·mol^{-1} was obtained at 300 K for [Mn(hfac)$_2$·**4**] and was already smaller than the theoretical one {$\chi_{mol}T = 0.125g^2S(S+1) = 0.125 \times 2 \times 2({}^2/_2({}^1/_2 + 1) + {}^5/_2({}^5/_2 + 1)) = 5.13$ emu·K·mol^{-1}}

calculated for two isolated $S = {}^1/_2$ spins and one $S = {}^5/_2$ spin in terms of the spin only equation. As the temperature was decreased, the $\chi_{mol}T$ value gradually decreased, reaching a plateau at 13 K, and rapidly decreased below 3 K. The $\chi_{mol}T$ value of 1.80 emu·K·mol^{-1} at the observed plateau is slightly smaller than the theoretical one (1.87) calculated for $S = {}^3/_2$. Equation 4 derived from an isosceles triangular three-spin model $\{H = -2J(S_{A1}S_M + S_MS_{A2} + \alpha S_{A1}S_{A2})\}$ with $S_{A1} = S_{A2} = {}^1/_2$ and $S_M = {}^5/_2$ was applied and fitted to the observed $\chi_{mol}T$ vs T plot for [Mn(hfac)$_2$·**4**] by means of a least-squares method.

$$\chi_{mol}T = \frac{Ng^2\beta^2T}{3k_B(T-\theta)}[15 + 52.5\exp(5J_{M-R}/k_BT) + 52.5\exp((7-2\alpha)J_{M-R}/k_BT) + 126\exp(12J_{M-R}/k_BT)]/[4 + 6\exp(5J_{M-R}/k_BT) + 6\exp((7-2\alpha)J_{M-R}/k_BT) + 8\exp(12J_{M-R}/k_BT)] \quad (4)$$

All the symbols have their usual meaning. The best-fit parameters are $J/k_B = -19.10 \pm 0.20$ K, $\alpha = 1.73 \pm 0.02$, $g = 1.96 \pm 0.01$, and $\theta = -0.11 \pm 0.02$ K, and the theoretical curve is represented by a solid line in Figure 4b.

(B-4) [Cu(hfac)$_2$·4]. A $\chi_{mol}T$ value of 1.22 emu·K·mol^{-1} was obtained at 300 K for [Cu(hfac)$_2$·**4**] and is close to the theoretical one (1.13 emu·K·mol^{-1}) calculated for three isolated $S = {}^1/_2$ spins in terms of the spin only equation. As the temperature was decreased, the $\chi_{mol}T$ value gradually increased, reached a maximum at 28 K, and rapidly decreased below 10 K. The observed maximum $\chi_{mol}T$ value of 1.36 emu·K·mol^{-1} is smaller than the theoretical one (1.87) calculated for $S = {}^3/_2$. The obtained $\chi_{mol}T$ vs T curve for [Cu(hfac)$_2$·**4**] was analyzed quantitatively on the basis of an isosceles triangular three-spin model. Equation 5 for three spins with $S_{A1} = S_{A2} = S_M = {}^1/_2$ was applied and fitted to the observed $\chi_{mol}T$ vs T plot for [Cu(hfac)$_2$·**4**] by means of a least-squares method.

$$\chi_{mol}T = \frac{Ng^2\beta^2T}{3k_B(T-\theta)}[15 + 1.5\exp(-(1+2\alpha)J_{M-R}/k_BT) + 1.5\exp(-3J_{M-R}/k_BT)]/[4 + 2\exp(-(1+2\alpha)J_{M-R}/k_BT) + 2\exp(-3J_{M-R}/k_BT)] \quad (5)$$

All the symbols have their usual meaning. Two sets of the best-fit parameters were (1) $J/k_B = 73.7 \pm 18.7$ K, $\alpha = -0.33 \pm 0.02$, $g = 1.97 \pm 0.02$, and $\theta = -4.34 \pm 0.18$ K and (2) $J/k_B = 9.10 \pm 1.23$ K, $\alpha = 14.9 \pm 1.4$, $g = 1.96 \pm 0.02$, and $\theta = -4.21 \pm 0.14$ K. The theoretical curve based on set 1 is presented by a solid curve in Figure 4c. The small values of θ suggest that the short contact between O(1) of the aminoxyl and C(18) of the pyridine ring within a dimer revealed by X-ray analysis is insignificant.

Discussion

Intramolecular Magnetic Couplings between Aminoxyls in 4 and Zinc Complex. The decrease in the hyperfine coupling with the aminoxyl nitrogen ($a_N/2$) from 5.6 to 5.1 G was observed in EPR spectra in fluid solution when **4** was converted to [Zn(hfac)$_2$·**4**]. The trend is in agreement with a similar decrease of $a_N = 10.5$ to 9.2 G when Zn(II) is complexed with **1**, and explained in terms of the shift of the spin density from the aminoxyl group to the pyridyl nitrogen by the electron-withdrawing Zn(II).[16] The observed increase in the dipolar coupling parameters in solid solution from $|D/hc| = 0.0054$ to 0.0094 cm^{-1} is in line with this interpretation; a mean distance between the two unpaired electrons becomes shorter when **4** is coordinated with Zn(II) to form [Zn(hfac)$_2$·**4**]. The exchange coupling between two aminoxyl units through the 2,2′-bipyridine ring was determined by the temperature dependence of the triplet signal intensities in EPR spectra. The J/k_B value for zinc complex [Zn(hfac)$_2$·**4**] is −24.3 K and slightly larger in magnitude than −19.3 for free **4**. The former value for [Zn(hfac)$_2$·**4**] is consistent with −28.2 K obtained from the susceptibility measurements. Strong intermolecular antiferromagnetic coupling did not allow us to determine the J/k_B value for **4** from SQUID susceptometric measurements. Actually, a short contact of 2.36 Å between the aminoxyl centers of a neighboring molecule was observed in the crystal structure of **4** revealed by X-ray analysis.

The dicarbene,[17] dinitrene,[18] and di(aminoxyl)[19] of the biphenyl-3,3′-diyl series are reported to have singlet ground states. The low-spin ground states are reasoned in terms of the tetramethyleneethane family of the non-Kekulé structures.[19] In other words, all belong to the disjoint system. The negative J_{R-R}/k_B values observed here serve as additional supports to this interpretation. The ring nitrogen of the 2,2′-dipyridine and the coordination with metal ions do not appear to perturb this trend. Furthermore, the magnetic coupling between the two aminoxyls appears to be slightly strengthened by the complexation with metal ions.

Competing Interactions in [Mn(hfac)$_2$·4] and [Cu(hfac)$_2$·4]. The Heisenberg spin Hamiltonian (eq 2) for an isosceles triangular three-spin model[9,10] gives energy diagrams consisting of one quartet state, two sextet states, and one octet state for [Mn(hfac)$_2$·**4**] and two doublet states and one quartet state for [Cu(hfac)$_2$·**4**]. A value of the small plateau, $\chi_{mol}T = 1.80$ emu·K/mol, observed below 13 K in the $\chi_{mol}T$ vs T plot for [Mn(hfac)$_2$·**4**], clearly indicates that the ground state is a quartet ($S = {}^3/_2$) and the α value in eq 4 should be less than 3.5 as suggested in the energy diagram. Actually, $\alpha = 1.73 \pm 0.02$ ($J_{R-R}/k_B = -32.9 \pm 0.3$ K) was obtained together with $J_{M-R}/k_B = -19.1 \pm 0.2$ K. The thermal behavior of $\chi_{mol}T$ above 230 K observed in the $\chi_{mol}T$ vs T plot for [Cu(hfac)$_2$·**4**] suggested that ferromagnetic interaction takes place within three spins. When the α value in eq 5 is greater than −0.5, two solutions are possible, one below and another above $\alpha = 1$. Actually, fitting of eq 5 to the experimental data for [Cu(hfac)$_2$·**4**] gave two solution sets, $J_{M-R}/k_B = 73.7 \pm 18.7$ K, $\alpha = -0.33 \pm 0.02$ ($J_{R-R}/k_B = -24.5 \pm 6.5$ K) and $J_{M-R}/k_B = 9.10 \pm 1.23$ K, $\alpha = 14.9 \pm 1.4$ ($J_{R-R}/k_B = 135 \pm 18$ K). Since the J_{R-R}/k_B value should not be very much different from those of -28.2 ± 0.1 K for [Zn(hfac)$_2$·**4**] and -32.9 ± 0.3 K for [Mn(hfac)$_2$·**4**], the former set was preferred for [Cu(hfac)$_2$·**4**]. Therefore, the ground state for [Cu(hfac)$_2$·**4**] is a quartet ($S = {}^3/_2$).

Comparison of the Magnetic Interactions in the Mixed-Ligand Complexes [M(hfac)$_2$·4], [M(hfac)$_2$·3], and [M(hfac)$_2$·1$_2$]. The sign of the exchange coupling J_{M-R} between the unpaired electrons of the magnetic metal ions and the aminoxyl radicals is governed by the overlap and orthogonality of the magnetic 3d orbital of the metal ion and the 2pπ orbital at the coordinating nitrogen atom of the ligand. The d_{xz} and/or d_{yz} orbitals of the former are π-type and can overlap with the 2pπ

(16) (a) Itoh, K. *Pure Appl. Chem.* **1978**, *50*, 1251. (b) Teki, Y.; Takui, T.; Kitano, M.; Itoh, K. *Chem. Phys. Lett.* **1987**, *142*, 181.

(17) Cazianis, C. T.; Eaton, D. R. *Can. J. Chem.* **1974**, *52*, 2454.
(18) Minato, M.; Lahti, P. M.; Willigen, H. V. *J. Am. Chem. Soc.* **1993**, *115*, 4532.
(19) Watanabe, T. M.Sc. Thesis, The University of Tokyo, 1990.
(20) Borden, W. T.; Iwamura, H.; Berson, J. A. *Acc. Chem. Res.* **1994**, *27*, 109.

Table 3. Magnetic Coupling Constants (J_{M-R}/k_B and J_{R-R}/k_B), Distances (r_{M-N}), and Dihedral Angles *ab* and *bc* for the Metal Complexes of $M(hfac)_2$ Coordinated with **4**, **3**, and **1**, Respectively

	4	**3**	**1**
	$Mn(hfac)_2$		
J_{M-R}/k_B (K)	-19.1 ± 0.2	-20.2	-12.4
J_{R-R}/k_B (K)	-32.9 ± 0.3		
r_{M-N} (Å)	2.24	2.21	2.27
ab (deg)[a]	17	21	1.7
bc (deg)[a]	5.9−5.7	6−5	17−15
	$Cu(hfac)_2$		
J_{M-R}/k_B (K)	73.7 ± 18.7	69.4	60.4
J_{R-R}/k_B (K)	-24.5 ± 6.5		
r_{M-N} (Å)	1.99, 2.00	1.98	2.05
ab (deg)[a]	33, 15	16	10
bc (deg)[a]	3.5−3.2, 3.7−3.4	3−0	25−24
	$Zn(hfac)_2$		
J_{M-R}/k_B (K)			
J_{R-R}/k_B (K)	-28.2 ± 0.1 (-24.3 ± 0.4)[c]		(-5.5)[b]
r_{M-N} (Å)	2.14	2.10	2.16
ab (deg[a]	16	19	0.7
bc (deg)[a]	7.5−5.8	5.3−1.8	19−14

[a] Dihedral angles *ab* and *bc* are shown in Figure 5. [b] Magnetic coupling constant between aminoxyls through zinc ion. [c] The value obtained by EPR measurements.

orbital at the nitrogen. The electron pairing should lead to antiferromagnetic interaction. When the magnetic orbital of the metal ion is $d_{x^2-y^2}$, it is orthogonal to the $2p\pi$ orbital at the nitrogen, and therefore the interaction becomes ferromagnetic.[1] This interpretation is in good agreement with the observed plus sign of J_{M-R} in the Cu(II) and minus sign in Mn(II) complexes as summarized in Table 3.

What about the magnitude of the exchange coupling? In principle, the $p\pi-d\pi$ overlap is considered to be dependent on the dihedral angle *bc* between the pyridine ring and the *xy* plane of the magnetic ions, and the distance between the two orbitals (see Figure 5). Such an angle dependence should be less obvious for the orthogonality of the $p\pi$ and $d\pi$ orbitals. Furthermore, both interactions should be dependent on the $p\pi$ spin density at the pyridyl nitrogen which is produced by spin polarization of the π-electrons by the aminoxyl radical center at position 4. Therefore, coplanarity of the plane of the aminoxyl unit and the pyridine ring should lead to the highest magnitude of the J_{R-M} values which would decrease with the increase in the dihedral angle *ab* in Figure 5.

The obtained values of J_{M-R}/k_B and J_{R-R}/k_B of metal ion−aminoxyl (M−R) and aminoxyl−aminoxyl (R−R), respectively, through the 2,2′-bipyridine ring for $[M(hfac)_2\cdot\mathbf{4}]$, distances between N of pyridine and metal ion, and dihedral angles of *ab* and *bc* are summarized in Table 3 together with those for the metal complexes coordinated with **1** and **3**.

When the J_{M-R}/k_B values for $[M(hfac)_2\cdot\mathbf{4}]$ are compared with those for $[M(hfac)_2\cdot\mathbf{3}]$ and $[M(hfac)_2\cdot\mathbf{1}_2]$, their magnitudes for $[M(hfac)_2\cdot\mathbf{4}]$ are close to those for $[M(hfac)_2\cdot\mathbf{3}]$ and considerably larger than those for $[M(hfac)_2\cdot\mathbf{1}_2]$. As listed in Table 3, bond lengths (r_{M-N}) between the nitrogen atom of the pyridine ring and the metal ions in $[M(hfac)_2\cdot\mathbf{4}]$, $[M(hfac)_2\cdot\mathbf{3}]$, and $[M(hfac)_2\cdot\mathbf{1}_2]$ are similar and dihedral angle *ab* (planes *a* and *b* in Figure 5) for $[M(hfac)_2\cdot\mathbf{4}]$ and $[M(hfac)_2\cdot\mathbf{3}]$ are even larger than the corresponding angles for $[M(hfac)_2\cdot\mathbf{1}_2]$. On the other hand, the dihedral angles *bc* between planes *b* and *c* for $[M(hfac)_2\cdot\mathbf{4}]$ and $[M(hfac)_2\cdot\mathbf{3}]$ are smaller than the ones for $[M(hfac)_2\cdot\mathbf{1}_2]$. This comparison suggested, therefore, that the magnitudes of magnetic coupling between the aminoxyl and the metal ion depend not only on the dihedral angle *ab* but also on *bc* and the latter is more effective.

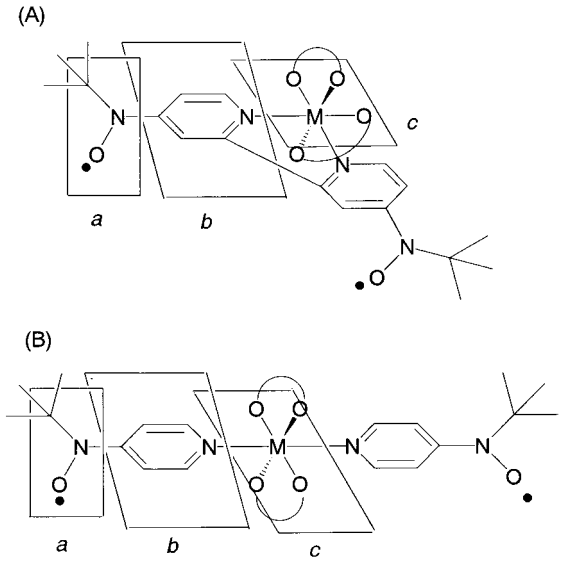

Figure 5. Illustrations of two parts of the dihedral angle *ab* and *bc* in (A) $[M(hfac)_2\cdot\mathbf{4}]$ and (B) $[M(hfac)_2\cdot\mathbf{1}_2]$; *a* for aminoxyl plane, *b* for pyridine ring, and *c* for plane of d_{xy} orbital of metal ion.

Conclusion

The magnetic properties of $[Mn(hfac)_2\cdot\mathbf{4}]$ and $[Cu(hfac)_2\cdot\mathbf{4}]$ were understood by using an isosceles triangular three-spin model. The values of magnetic coupling between two aminoxyls through the 2,2′-bipyridine ring, $J_{R-R}/k_B = -32.9 \pm 0.3$ and -24.5 ± 6.5 K for $[Mn(hfac)_2\cdot\mathbf{4}]$ and $[Cu(hfac)_2\cdot\mathbf{4}]$, respectively, are close to those, $J_{R-R}/k_B = -19.3 \pm 0.5$ and -28.2 ± 0.1 (-24.3 ± 0.4) K, for **4** and $[Zn(hfac)_2\cdot\mathbf{4}]$, respectively. The signs of the magnetic coupling (J_{M-R}/k_B) between aminoxyl and metal ion are the same as those for the corresponding 1:1 and 1:2 complexes with **2** and **3**, respectively; antiferromagntic for manganese(II) and ferromagnetic for copper(II) complex. The magnitudes of the coupling for 2,2′-bipyridine complexes are larger than those for the corresponding pyridine complexes.

Acknowledgment. This work was supported by a Grant-in-Aid for COE Research "Design and Control of Advanced Molecular Assembly Systems" from the Ministry of Education, Science, Sports and Culture, Japan (08CE2005).

Supporting Information Available: ORTEP drawings of the molecular structures for **4** and $[Zn(hfac)_2\cdot\mathbf{4}]$, Figures S1 and S2, respectively. EPR spectra in frozen toluene solutions and the intensity (*I*) vs *T* plots for **4** and $[Zn(hfac)_2\cdot\mathbf{4}]$, Figures S3 and S4, respectively. This material is available free of charge via the Internet at http://pubs.acs.org.

IC991205F